Inorganica Chimica Acta 499 (2020) 119176

Contents lists available at ScienceDirect

Inorganica Chimica Acta

journal homepage: www.elsevier.com/locate/ica

Research paper

A rare flattened tetrahedral Mn(II) salen type complex: Synthesis, crystal structure, biomimetic catalysis and DFT study

Saikat Banerjee[a], Pravat Ghorai[a], Papiya Sarkar[b], Anangamohan Panja[c,d], Amrita Saha[a,*]

[a] Department of Chemistry, Jadavpur University, Kolkata 700032, India
[b] Chemistry and Biomimetics Group, CSIR-Central Mechanical Engineering Research Institute, M. G. Avenue, Durgapur 713209, India
[c] Department of Chemistry, Panskura Banamali College, Panskura RS, WB 721152, India
[d] Department of Chemistry, Gokhale Memorial Girls' College, 1/1 Harish Mukherjee Road, Kolkata 700020, India

ARTICLE INFO

Keywords:
Mn(II) salen type complex
Crystal structure
Spectroscopic studies
Phenoxazinone synthase like activity
Theoretical calculations

ABSTRACT

A new flattened tetrahedral high spin Mn(II) complex (**1**) has been synthesized using N_2O_4 donor Schiff base ligand. Complex **1** was characterized by X-ray diffraction and various spectroscopic techniques. For further understanding of electronic structure of the complex, DFT calculations and electrochemical studies have been performed. This is a rare example of a flattened tetrahedral Mn(II) salen type Schiff base complex. High-spin d^5 configuration of the metal center provides no crystal-field stabilization energy to the system and that is the main reason behind the significant deviation of this salen-type ligand from planarity. Notably, the propylenic linker in the ligand provides adequate flexibility so that such an uncommon binding mode of the salen type Schiff base ligand becomes possible. Complex **1** exhibits excellent catalytic property towards oxidation of *o*-aminophenols in aerobic condition. Detailed kinetic investigations together with the mass spectrometry studies reveal several important information relating to biomimetic catalytic activity of the present complex.

1. Introduction

Manganese is the 12th most naturally occurring trace metal found in the living systems. Coordination chemistry of manganese is driven by a part of its occurrence in the active sites of several enzymes in the biological systems [1–4]. For example, in photosystem-II (PS-II), manganese centers constitute oxygen evolving complex (OEC) which photolytically oxidizes water to oxygen. In the active site structures of Mn containing catalase [5–7] and peroxidase, the manganese centers are found to coordinate with N or O donor ligands [8,9]. It is clear that nature has chosen Mn in the active site of different metalloenzymes due to its rich redox properties and possibilities of presence of Mn ions in different geometries and stable oxidation states. These enzymatic activities of Mn inspired us to use its model complexes for selective oxidation of organic molecules. It is important to mention that synthesis of biologically-compatible, environment-friendly and energetically-efficient metal complexes is a challenging task for the development of new chemicals for industrial processes and subsequently facilitating the advancement of science in different fields. Oxidation process plays a crucial role in organic reaction for the synthesis of several valuable organic compounds in the fields of pharmaceuticals, agrochemicals, etc. [10–12]. Although in chemical industries mainly molecular oxygen is used as a primary oxidant, [13–17] direct oxidation of small organic molecules by molecular oxygen is still difficult because of its spin restriction that reduces its reactivity severely with ending up of poor yield [18–21]. In this connection phenoxazinone synthase (PHS) needs special mention for its biological importance, which is a penta copper oxidase that efficiently activates molecular dioxygen at ambient condition to catalyze the oxidative coupling of two molecules of a substituted *o*-aminophenol to the phenoxazinone chromophore in the final step for the biosynthesis of actinomycin D [22,23]. Actinomycin D is an aromatic heterocyclic natural product which is clinically used for treatment of choriocarcinoma, wilms tumors, rhabdomyosarcoma, and Kaposi's sarcoma [24]. So, it is important to develop metal complexes which can efficiently mimic PHS by oxidizing *o*-aminophenol to 2-aminophenoxazin-3-one chromophore [25].

On the other hand, Schiff base ligands are classical chelating ligands which are vigorously used to understand molecular processes occurring in biochemistry, material science, catalysis, encapsulation, activation, transport and separation phenomena, hydrometallurgy, etc. [26,27]. Their ease of synthesis and reactivity with almost all metal ions present in the periodic table make them suitable synthons for the development of coordination chemistry. Literature has witnessed rich coordination chemistry involving H_2L (Scheme 1) ligand with reports of numerous

* Corresponding author.
E-mail address: amritasahachemju@gmail.com (A. Saha).

https://doi.org/10.1016/j.ica.2019.119176
Received 27 July 2019; Received in revised form 26 September 2019; Accepted 26 September 2019
Available online 27 September 2019
0020-1693/

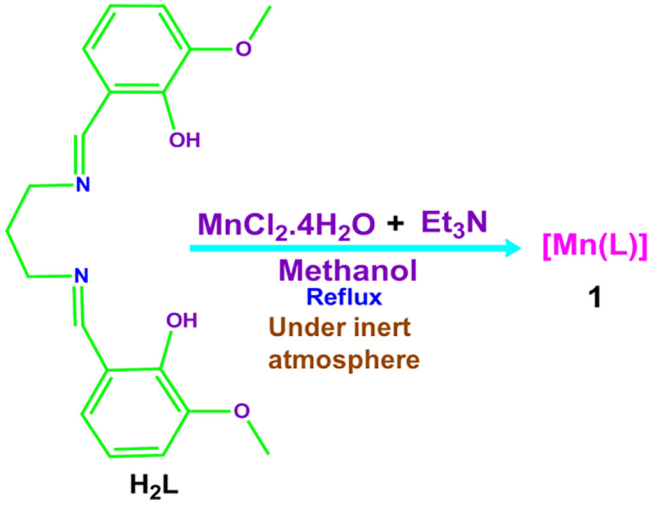

Scheme 1. The route to the syntheses of complex **1**.

mono-, di-, tri-, tetra- and polynuclear complexes having 3d and 4d metals [28,29]. A close inspection of the manganese chemistry clearly suggests that in all cases Mn(II) salt upon reaction with different types of salen ligands produce Mn(III) complexes where Mn(II) centers undergo aerial oxidation [29]. The enormous applicability of such Mn(III) complexes in diverse oxidation reactions is well known, and the redox flexibility between the Mn(III) and Mn(II) plays the crucial role in those redox processes. Interestingly, the crystallographic information of Mn (II) salen type Schiff base complex is rarely available in the literature [30] that motivated us to prepare Mn(II) complex using salen type ligand H_2L as that could provide significant information of role of the manganese center in the oxidation reactions. With this aim, we are first time reporting here the crystallographic information of flatten tetrahedral Mn(II) salen type Schiff base complex [Mn(L)] (**1**). It is also important to mention that although various Mn(III) octahedral complexes are known in literature, a few examples are known to have other coordination geometries [31]. Complex **1** has been characterized by various spectroscopic techniques and structure has been elucidated by X-ray crystallography. UV–Vis spectrum and X-ray data are further verified using DFT and TDDFT calculations. Furthermore, the oxidation of *o*-aminophenols catalyzed by the synthesized complex has been explored.

2. Experimental

2.1. Materials and physical measurements

All reagent or analytical grade chemicals and solvents were purchased from commercial sources and used without further purification.

Elemental analysis for C, H and N was carried out using a Perkin–Elmer 240C elemental analyzer. Infrared spectra (400–4000 cm^{-1}) were recorded from KBr pellets on a Nicolet Magna IR 750 series-II FTIR spectrophotometer. Absorption spectra were measured using a Cary 60 spectrophotometer (Agilent) with a 1-cm-path-length quartz cell. The electrochemical data of complex **1** have been recorded in methanol containing 0.1 M tetraethylammonium perchlorate as a supporting electrolyte in a conventional three electrode configuration using a Pt disk working electrode, Pt auxiliary electrode and Ag/AgCl reference electrode using a PC-controlled PAR model 273A electrochemical system. Electron spray ionization mass (ESI-MS positive) spectra were recorded on a MICROMASS Q-TOF mass spectrometer. Electron paramagnetic resonance (EPR) spectra were recorded in standard quartz EPR tubes using a Varian E-109C spectrometer.

Table 1
Crystal parameters and selected refinement details for complex **1**.

Complex	**1**
Empirical formula	$C_{19}H_{20}MnN_2O_4$
Formula weight/g mol^{-1}	395.31
Temperature/K	293(2)
Crystal system	Orthorhombic
Space group	*Pbcn*
a/Å	24.7944(10)
b/Å	8.0362(3)
c/Å	8.6956(4)
α/°	90
β/°	90
γ/°	90
Volume/$Å^3$	1732.62(12)
Z	4
ρ_{calc} g/cm^3	1.515
μ/mm^{-1}	0.790
F(0 0 0)	820.0
Crystal size/mm^3	0.2 × 0.1 × 0.06
2θ range for data collection/°	3.286–54.32
Index ranges	$-31 \le h \le 31,\ -10 \le k \le 10,\ -11 \le l \le 11$
Reflections collected	25,178
Independent reflections	1926 [R_{int} = 0.0362, R_{sigma} = 0.0178]
Data/restraints/parameters	1926/0/120
Goodness-of-fit on F^2	1.061
Final R indexes [I > 2σ (I)]	R_1 = 0.0477, wR_2 = 0.1495
Final R indexes [all data]	R_1 = 0.0585, wR_2 = 0.1598
Largest diff. peak/hole/e $Å^{-3}$	0.60/−0.43

2.2. X-ray crystallography

Single crystal X-ray data of complex **1** was collected on a Bruker SMART APEX-II CCD diffractometer using graphite monochromated Mo Kα radiation (λ = 0.71073 Å) at room temperature. Data processing, structure solution, and refinement were performed using Bruker Apex-II suite program. All available reflections in $2\theta_{max}$ range were harvested and corrected for Lorentz and polarization factors with Bruker SAINT plus [32]. Reflections were then corrected for absorption, inter-frame scaling, and other systematic errors with SADABS [33]. The structure was solved by the direct methods and refined by means of full matrix least-square technique based on F^2 with SHELX-2017/1 software package [34]. All the non-hydrogen atoms were refined with anisotropic thermal parameters. C–H hydrogen atoms were inserted at geometrical positions with U_{iso} = 1.2U_{eq} to those they are attached. Crystal data and details of data collection and refinement for **1** are summarized in Table 1.

2.3. Synthesis of Schiff base ligand (H_2L = *N,N′-bis(3-methoxysalicylidene)propylene-1,3-diamine)*

The tetradentate Schiff base ligand (H_2L) was prepared by the well-known method described in literature [28,29,35]. Briefly, a mixture of *o*-vanillin (4.0 mmol, 0.608 g) and 1,3-diaminopropane (2.0 mmol, 0.148 g) in 25 mL methanol was heated to reflux for 2 h. The resulting light yellow colored Schiff base ligand (H_2L) was directly used for the following reaction.

2.4. Preparation of [Mn(L)] (1)

A methanolic solution (2 mL) of manganese chloride tetrahydrate (1.0 mmol, 0.198 g) was added drop wise to 20 mL methanolic solution of H_2L (1.0 mmol) followed by addition of triethylamine (2.0 mmol, ~0.4 mL) and the resultant reaction mixture was heated to reflux for 4 h under nitrogen atmosphere. The solution was then cooled and filtered. Light green colored needle shaped crystals resulted from the slow evaporation of methanolic solution of the complex at room temperature. Yield: 0.2963 g (75%). Anal. Calc. for $C_{19}H_{20}MnN_2O_4$: C 57.73%;

H 5.10%; N 7.09%. Found: C 57.25%; H 5.01%; N 6.98%. IR (cm^{-1}, KBr): ν(C=N) 1627m; ν(C–N) 1220s; ν(C–H) 739 s. UV–Vis, λ_{max} (nm), (ε ($dm^3\,mol^{-1}\,cm^{-1}$)) in methanol: 280 (55262) and 370 (14120).

2.5. Computational method

All computations were performed using the GAUSSIAN09 (G09) [36] software. Full geometry optimizations were carried out using the density functional theory method at the B3LYP level [37,38] for the complex **1**. The coordinates obtained from single crystal X-ray diffraction data was used for optimization using the lanL2DZ effective potential (ECP) set of Hay and Wadt [39–41] for manganese atom and the standard 6-31 + G(d) basis set for C, H, N and O atoms, respectively [42,43]. To get local minima and only positive eigen values of optimized geometries, the vibrational frequency calculation were carried out. Time-dependent density functional theory (TDDFT) was computed [44,45] in methanol using conductor-like polarizable continuum model (CPCM) [46–49] with the same B3LYP level and basis sets to get vertical electronic excitations. GAUSSSUM 3.0 [50] was used to calculate the percentage contributions of ligand, coligand and metal ion to each molecular orbital.

2.6. Hirshfeld surface analysis

Hirshfeld surface analysis have been done using Crystal Explorer version 3.1 [51]. The normalized contact distance (d_{norm}) based on d_i and d_e has been determined by the given equation where r^{vdW} is the van der Waals (vdW) radius of the appropriate atom internal or external to the surface.

$$\text{dnorm} = \frac{(d_i - r_i^{vdW})}{r_i^{vdW}} + \frac{(d_e - r_e^{vdW})}{r_e^{vdW}}$$

d_{norm} becomes negative for shorter contacts than vdW separations and becomes positive for contacts greater than vdW separations, and is displayed using a red–white–blue color scheme, where red highlights shorter contacts, white is used for contacts around the vdW separation, and blue is for longer contacts [52].

2.7. Biomimetic catalysis (catalytic oxidation of o-aminophenols)

Oxidation of *o*-aminophenols catalysed by the complex was examined by the reacting 1.0×10^{-5} M dioxygen-saturated methanolic solutions of the complex with 10^{-2} M solution of *o*-aminophenols at 25 °C. The progress of the reactions was monitored by the successive increase in absorbance band of phenoxazinone chromophore using literature reported extinction coefficients values [53]. To evaluate the rate dependency of the reaction on *o*-aminophenols and to evaluate various kinetic parameters like V_{max}, K_M, k_{cat}, 2.0×10^{-5} (M) solution of the complex was mixed with various concentration of the substrates maintaining minimum 10 folds excess to that of catalyst to retain the pseudo-first-order condition. Rate of a reaction was evaluated from the initial rate method, and the average initial rate over three independent measurements was recorded.

3. Results and discussion

3.1. Preparation of Schiff base ligand (H_2L) and complex 1

The ligand H_2L was synthesized by the condensation reaction of 1,3-diaminopropane and *o*-vanillin in a 1:2 M ratio in methanol following the standard procedure [28,29,35]. The ligand possesses six potential donor sites; two azomethine nitrogen atoms, two phenolic oxygen atoms and two oxygen atoms of methoxy groups. Salen type ligands by reacting with Mn(II) salts in aerobic conditions exclusively produced Mn(III) complexes in which Mn(II) center is air oxidized. Interestingly, in the present endeavor, $MnCl_2{\cdot}4H_2O$ upon reaction with H_2L in presence of Et_3N in 1:1:2 M ratio in methanol afforded the mononuclear complex [Mn(L)] (**1**) strictly under inert atmosphere in which oxidation state of manganese is +II (Scheme 1). It is important to note that only one report of crystallographically characterized Mn(II) complex with salen type ligands is available in the literature, and thereby present report could be further helpful in the better understating of manganese salen chemistry and would motivate the researchers working in this field to isolate and structurally characterized similar complexes of high importance.

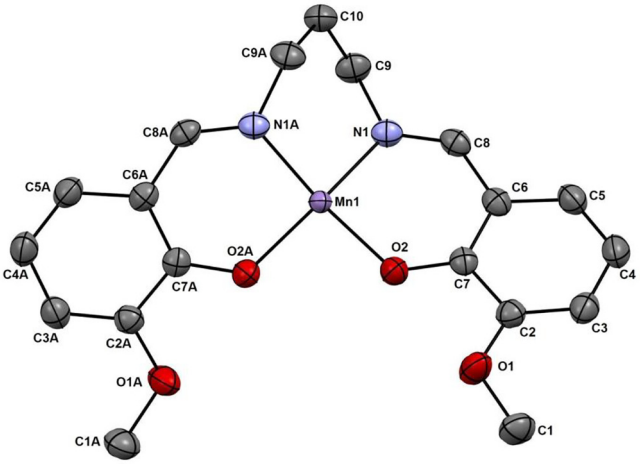

Fig. 1. Ortep view of complex **1**. Atoms are shown as 30% thermal ellipsoids. H atoms are omitted for clarity. [Symmetry Code: A = −x, y, 1/2 − z].

3.2. Crystal structure description of [Mn(L)] (1)

The molecular structure of **1** is shown in Fig. 1. The selected bond distances and angles are given in Table 2.

The X-ray data reveal that complex **1** crystallizes in the orthorhombic *Pbcn* space group. The Mn(II) complex is a mononuclear compound and the metal center is tetra coordinated, where the coordination numbers are satisfied by a pair of imine nitrogen atoms (N1 and N1A) and phenoxido oxygen atoms (O2 and O2A) provided by the deprotonated tetradentate Schiff base ligand in order to adopt distorted tetrahedral geometry. The dipositive charge of the manganese ion is satisfied by two phenoxido oxygen atoms. The structure of the complex possesses 2-fold rotation axis where the Mn(II) ion sits on an inversion centre. The angle between two planes i.e. N1–Mn1–O2 and N1A–Mn1–O2A is 39.53° implying flatten tetrahedral geometry. The Mn–N (1.938(2)Å) and Mn–O (1.907(2) Å) bond distances are relatively shorter with those found in the similar tetrahedral structures reported earlier [54]. However, the EPR spectrum of the complex at liquid nitrogen temperature shows characteristic six-line spectrum at g = 2.04, ensuring the +II oxidation state of manganese (Fig. 2). The bite angles around manganese (N(1)–Mn(1)–N(1A) = 92.41(15)°, N(1A)/N(1)–Mn(1)–O(2)/O(2A) = 93.98(7)° and O(2)–Mn(1)–O(2A) = 93.68(14)°

Table 2
Selected bond lengths (Å) and bond angles (°) for complex **1**.

	X-ray	Calculated
Mn1–N1	1.938	1.9552
Mn1–N1A	1.938	1.9569
Mn1–O2	1.907	1.8365
Mn1–O2A	1.907	1.8365
C9–C10–C9A	115.6	111.32
N1–Mn1–O2	94.0	91.71
N1–Mn1–N1A	92.4	88.97

[Symmetry Code: A = −x, y, 1/2 − z].

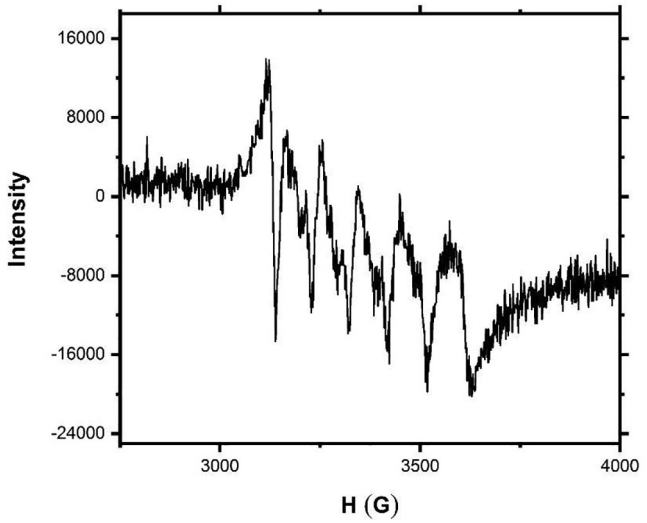

Fig. 2. X-band EPR spectrum of complex **1** at 77 K.

respectively) deviate from the ideal tetrahedral values. The two six-membered MnC_3NO chelate rings are not planar. The dihedral angle between two chelate rings is 42.72°. The propylenic part of the Schiff base, N1–C9–C10–C9A–N1A, is to some extent puckered due to the sp^3 hybridization of the saturated portion of the chelating ligand. The bond angle (C9–C10–C9A, 115.68(6)°) deviates appreciably from its ideal value.

In complex **1**, one dimensional self-assembly along the *c* axis is observed, supported by significantly strong hydrogen bonds between oxygen atom of methoxy group and H-atom of azomethine group. This H-bonding distance is around 2.717 Å. Also, an intermolecular H-bonding interaction between same azomethine H atom and the phenolic oxygen from the neighboring molecule with donor-acceptor distance of 2.692 Å has been observed (Fig. 3).

It is important to note that salen type ligands generally coordinate the metal centers in equatorial positions with minimal deviation from planarity because of its inherent righty. Notably, all the reported Mn (III) complexes with H_2L ligand are hexa-coordinated with octahedral geometry in which the ligand coordinates the metal center at equatorial positions as expected [55]. However, in the present case it is significantly deviated from planarity resulting in an outcome of flattened tetrahedral geometry, which is extremely rare in the coordination chemistry with salen type ligands. Close inspection of the crystal structure reveals that the propylenic linker in the ligand provides adequate flexibility so that such an uncommon binding mode of the salen type Schiff base ligand become a reality.

3.3. Spectroscopic study

Besides elemental analysis, ligand (H_2L) and complex **1** were initially characterized by IR spectroscopy. A strong and sharp band appeared at 1629 and 1627 cm^{-1}, respectively for the ligand (H_2L) and complex **1** due to azomethine ν(C=N) (Figs. S1 and S2). Complex **1** exhibits two absorption bands around 280 nm and 370 nm (Fig. S3). These absorption bands can be assigned to $\pi \rightarrow \pi^*$ and $n \rightarrow \pi^*$ transitions of the Schiff base ligand. The spectroscopic values agree with the literature values for distorted tetrahedral Mn(II) compounds [56]. The magnetic moment $\mu_{eff.}$ is around 5.78 BM at 300 K as expected for an isolated $S = 5/2$ Mn(II) monomer.

3.4. DFT study

The coordinates obtained from single crystal X-ray diffraction data of complex **1** was used for optimization using DFT/B3LYP method. Bond lengths and angles obtained from the DFT optimized structure of the complex **1** show well agreement with that of X-ray structures (Table 2).

Mulliken charge distribution shows that positive charge on metal atom i.e. 1.496537. Mulliken charge distribution of complex **1** is depicted in Table S1. Energy (eV) of some selected molecular orbitals of complex **1**, key electronic transitions and composition of M.O.s of some selected ones are presented in Tables S2 and S3, respectively. Contour plots of some selected M.O.s are given in Fig. S4 and S5. The energies of HOMO and LUMO are −2.5 eV (α-spin), −5.1 eV (β-spin) and −1.97 eV (α-spin), −2.12 eV (β-spin) respectively.

From DFT study it has been found that molecular orbitals (M.O.s)

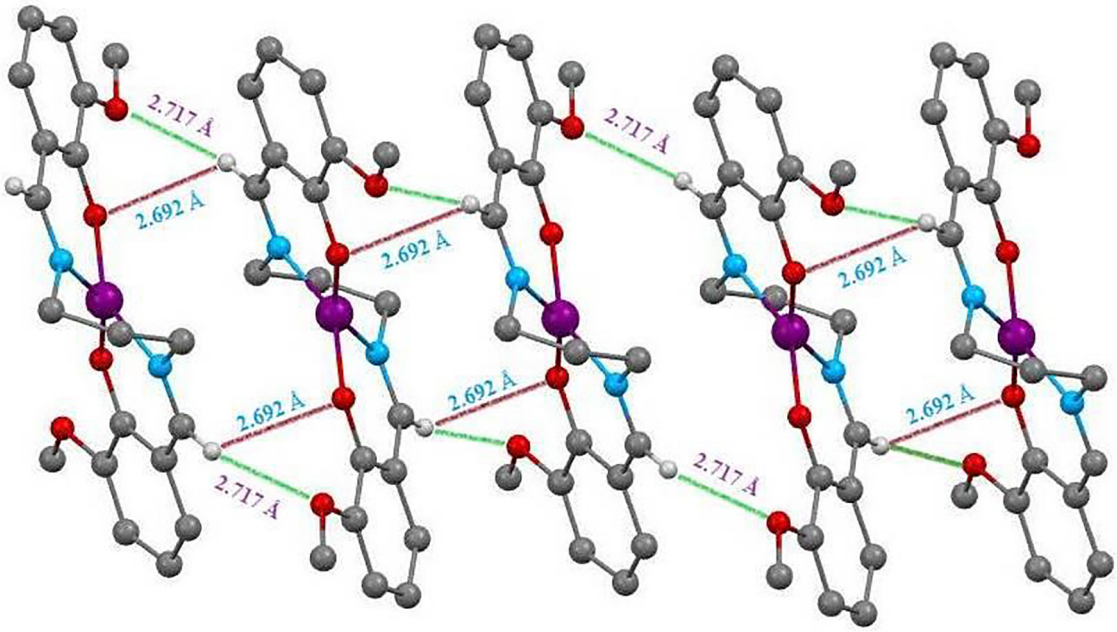

Fig. 3. 1D supramolecular architecture of complex **1** showing intermolecular hydrogen bonding interactions along the *b* axis. Hydrogen atoms of least interest are omitted for clarity.

HOMO to HOMO − 5 (both α-spin and β-spin) have major contribution from ligand i.e. these orbitals are rich in π(L) character. Whereas LUMO + 4 (α-spin), LUMO to LUMO + 3 (β-spin) molecular orbitals have major contribution from dπ of Mn centre. LUMO (α-spin), LUMO + 2 (α-spin) and LUMO + 5(α-spin) have significant contributions from ligand π*(L) site. LUMO + 1 (α-spin), LUMO + 1 (β-spin) and LUMO + 5 (β-spin) have contributions from both metal and ligand in comparable extend.

3.5. TDDFT study

For better understanding of electronic transition TDDFT calculations were performed using B3LYP/CPCM method using same basis sets in methanol solvent. The calculated electronic transitions along with the calculated Oscillator Strength (f) are given in Table S3. Complex **1** shows intense absorption band for ligand based $\pi \rightarrow \pi^*$ and $n \rightarrow \pi^*$ transitions around 280 nm and 370 nm, respectively. The bands at 280 nm and 370 nm are theoretically assigned as the following excitations at 4.24 eV (λ = 292.72 nm, f = 0.0188), 4.22 eV (λ = 293.75 nm, f = 0.0473) and 3.41 eV (λ = 363.05 nm, f = 0.0688), 3.30 eV (λ = 375.25 nm, f = 0.0083), respectively and these are due to the contribution of HOMO(β) → LUMO + 2(β) (73%), HOMO − 1(β) → LUMO + 2(β) (54%) and HOMO − 1(α) → LUMO + 5(α) (51%), HOMO − 3(α) → LUMO(α) (49%) transitions.

3.6. Hirshfeld surface analysis

Supramolecular interactions are further investigated using Hirshfeld Surface analysis. Complex **1** is mapped over d_{norm} (range of −0.1 to 1.5 Å), shape index (range of −1.0 to 1.0 Å) and curvedness (range of −4.0 to 0.4) respectively and presented in Figs. S6 and S7, respectively.

During mapping surfaces are kept transparent for visualization of different supramolecular interactions. For Complex **1**, H-bonding interactions between the O atom of methoxy group and H atoms of the imine group has been predominantly found as bright red area in the Hirshfeld surfaces. Other longer and weaker interactions appeared as light colour in the surfaces. Fingerprint plots consist of all type of intermolecular interactions. So, fingerprint plots need to be decomposed to have idea of individual contacts. In the decomposed fingerprint plot, complementary regions are obtained where one molecule acts as a donor (de > di) (bottom left of fingerprint plot) and the other as an acceptor (de < di) (bottom right of fingerprint plot). For complex **1**, O···H/H···O and H···H interactions comprise 20.60% and 46.80% of the total Hirshfeld surface. O···H interactions comprise around 11.3% of the total Hirshfeld surface and represented by a spike (d_i = 1.025 Å, d_e = 1.35 Å) in the bottom left (donor) area. Whereas H···O interactions comprise around 9.3% of the total Hirshfeld surface and represented by a spike (d_i = 1.355 Å, d_e = 1.025 Å) in the bottom right (acceptor) region (Fig. S8).

3.7. Electrochemical study

The electrochemical behaviour of the complex has been checked in methanol in the presence of 0.1 M tetraethylammonium perchlorate as a supporting electrolyte at ambient temperature. In order to get more insight into the real electronic states of the complex and its sensitivity towards the molecular dioxygen, the electrochemical studies have been performed both in nitrogen atmosphere and in aerobic condition, and the cyclic voltammograms of complex **1** are displayed in Fig. S9, in which the potentials are referenced to the standard Ag/AgCl electrode. When the cyclic voltammogram was recorded in nitrogen atmosphere, an irreversible oxidation at 1.28 V was observed, which can be assigned to the oxidation of Mn(II) to Mn(III). Moreover, a reductive response at −1.38 V was observed, which could be due to the reduction of Mn(III) to Mn(II) (Fig. S9a). These potential values suggest that both after oxidation and reduction the electrochemically generated species had been modified chemically. Huge structural difference of the Mn centre in different oxidation states is presumably responsible for such electrochemical events. Interestingly, when the cyclic voltammogram was recorded in aerobic condition, only an irreversible reduction response at −1.25 V was observed which is comparable to the cathodic response when the electrothermal study was conducted in nitrogen atmosphere (see Fig. S9b). Similar electrochemical response was also observed in recently reported Mn(III)-salen type complex, [29h] but only difference is that in the present case the reduction is less favourable, which can be realised from the fact that the high reorganisation energy required for the structural change at the metal centre in both oxidation and reduction processes brings lower redox flexibility in the present system. Furthermore, absence of any oxidative response in aerobic condition indicates that this Mn(II)-salen type complex is highly susceptible to aerial oxidation leading the fast conversion to Mn(III) species, even faster than the electrochemical time scale.

3.8. Functional model for phenoxazinone synthase like activity

3.8.1. Spectrophotometric study

The phenoxazinone synthase like activity of the complex was examined by monitoring the oxidation of *o*-aminophenol (OAPH) spectrophotometrically in dioxygen-saturated methanol as both complex and substrate are well soluble in methanol. Catalytic oxidation of *o*-aminophenol (OAPH) was studied in absence of added base to avoid autoxidation of the substrate by air. To investigate the catalytic efficiency of the complex, spectral scan of the resultant mixture of 1×10^{-5} M methanolic solution of complex **1** and 0.01 M OAPH was performed in 5 min time interval at 25 °C under aerobic condition. As can be seen from Fig. 4, the characteristic absorbance band of phenoxazinone chromophore ca. at 433 nm gradually increases upon successive catalytic oxidation of *o*-aminophenol (OAPH) to 2-aminophenoxazin-3-one.

A blank experiment has been performed in absence of the complex **1** under identical condition, which does not result any significant enhancement in the band intensity ca. at 433 nm. The result of the experiment implies that complex **1** is catalytically efficient to oxidize OAPH to 2-aminophenoxazin-3-one under aerobic condition. In order to understand the degree of catalytic efficiency of complex **1**, detail kinetic studies were performed at 25 °C. For this purpose, 1×10^{-5} M methanolic solution of complex **1** was reacted with various

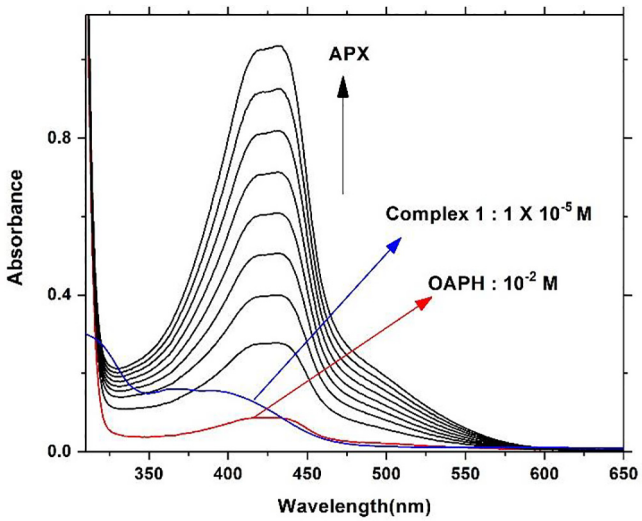

Fig. 4. UV–Vis spectral scans showing the increase in phenoxazinone chromophore band at 433 nm after the addition of *o*-aminophenol (10^{-2} M) to a solution of complex **1** (1×10^{-5} M) in methanol at 25 °C. The spectra were recorded in 5 min time interval.

concentration of the substrate maintaining at least 10 folds excess with respect to the catalyst used to maintain pseudo first order reaction condition. For each kinetic measurement time scan at the maximum band (433 nm) of 2-aminophenoxazin-3-one was carried out for a period of 10 min using particular substrate ratio to that of the complex. The initial rate was determined by linear regression from the slope of the absorbance versus time, and each experiment was performed thrice and average values were noted. The initial rate of the reactions verses concentrations of the substrate plot shows rate saturation kinetics as depicted in Fig. S10. These kinetic data can be fitted to Michaelis–Menten model to get different kinetic parameters like V_{max}, K_M, and k_{cat}. These can also be determined by linearization of Michaelis–Menten equation which gives double reciprocal Lineweaver-Burk plot (Fig. S11). Michaelis binding constant (K_M) and V_{max} were calculated to be $(1.09 \pm 0.35) \times 10^{-2}$ M and 6.14×10^{-8} M s^{-1}, respectively. The turnover number (k_{cat}) is calculated by dividing the V_{max} by the concentration of the complex used, and is found to be 22.10 h^{-1}.

A reasonable numbers of model complexes are known in the literature mimicking the function of phenoxazinone synthase to better understand the possible mechanistic pathway and their catalytic efficiency. In order to increase the scope for wider perspective, we also examined the detailed catalytic activity using 2-amino-5-methylphenol (5-MeOAPH) as a substrate to get further insights into the reactive intermediates and the mechanistic details of the catalytic reactions and finally to examine the effect of substitution on the catalytic reactivity. The spectral profile shown in Fig. 5 discloses the catalytic oxidation of 2-amino-5-methylphenol in aerobic condition leading to cumulative increase of the product 2-amino-4,4a-dihydro-4a-7-dimethyl-3*H*-phenoxazine-3-one. Detailed kinetic analysis further gives us the values $K_M = (1.50 \pm 0.30) \times 10^{-2}$ M $V_{max} = (8.58 \pm 1.21) \times 10^{-7}$ M s^{-1} and $k_{cat} = 30.9$ h^{-1}.

3.8.2. ESI mass spectral study

Mass spectrometry is considered one of the most useful technique as that could provide significant information regarding the important intermediates of a chemical reaction from which one can frame the most possible mechanistic pathway of a catalytic reaction. Accordingly, the ESI (positive) mass spectra of compound **1** alone and in the presence of excess OAPH after 15 min of mixing were recorded, and the spectra are depicted in Figs. S12 and S13 (expanded view in Fig. S14), respectively. In the mass spectrum of complex **1**, the base peak at m/z = 395.04 is nicely matched with $[Mn^{III}(L)]^+$ cationic species (calculated m/z = 395.08).

When the mass spectrum was carried out in presence of excess substrate, the base peak was found at m/z = 365.10, which can be assigned to the sodium salt of ligand H_2L (calculated m/z = 365.15). The peak at m/z = 343.12 can be assigned to the protonated Schiff base H_2L (calculated m/z = 343.16). The second most abundant peak at m/z = 244.05 is a molecular ion peak of product 2-aminophenoxazin-3-one along with a solvated methanol (calculated m/z = 244.08). Another product related peak at m/z = 267.10 is nicely matched with sodium adduct of 2-aminophenoxazin-3-one together with a solvent methanol molecule. The peak at m/z = 110.02 is nothing but a protonated substrate of OAPH. One of the moderately abundant peak at m/z = 215.04 is quite interesting as the isotopic distribution patterns match well with the protonated intermediate II-B (calculated m/z = 215.08) as shown in scheme 2. Furthermore, a peak at m/z = 213.03 is also a product related peak as that matched with the protonated species of 2-aminophenoxazin-3-one (calculated m/z = 213.06). Integrity of the original complex was ensured by the presence of two minor peaks at m/z = 395.03 and 418.02 as these are well matched with the monocationic species of compositions $[Mn(L)]^+$ (calculated m/z = 395.08) and $[NaMn(L)]^+$ (calculated m/z = 418.07), respectively (see Fig. S14).

Further inspection of the mass spectrum (Fig. S14) discloses several minor peaks which are related to the intermediates in the course of production of 2-aminophenoxazin-3-one. The peaks at m/z = 485.24 and 507.22 are nicely matched with dioxygen bound manganese species of compositions $[KMn(L)(HO_2)(H_2O)]^+$ (calculated m/z = 485.05) and $[NaKMn(L)(O_2)(H_2O)]^+$ (calculated m/z = 507.03), respectively, clearly indicating the interaction of dioxygen with the metal centre at the catalytic cycle. The peak at m/z = 523.19 is a substrate bound species of formula $[HMn(L)(OAPH)(H_2O)]^+$ that suggests binding of the substrate to the metal centre during the catalytic oxidation of the substrate, which is consistent with the rate saturation kinetics.

Similarly, the mass spectrum (Fig. S15) of the complex in presence of substrate 2-amino-5-methylphenol is also quite informative. The base peak at m/z = 124.07 is matched with the protonated species of substrate 2-amino-5-methylphenol (calculated m/z = 124.08). A product related peak was found at m/z = 243.09 (Fig. S15) as it matched with the protonated species of the product 2-amino-4,4a-dihydro-4a-7-dimethyl-3*H*-phenoxazine-3-one (calculated m/z = 243.11). Another minor peak at m/z = 567.14 (Fig. S16) is also interesting as it agrees well with the monocationic species of the complex-substrate adduct of composition $[Mn(L)(5\text{-Me-OAP})(MeOH)(OH_2)]^+$ (calculated m/z = 567.18), which clearly justifies that effect of methyl substitution does not inhibit the formation of a stable complex substrate adduct. Isotopic distribution of key m/z values and their simulated pattern are

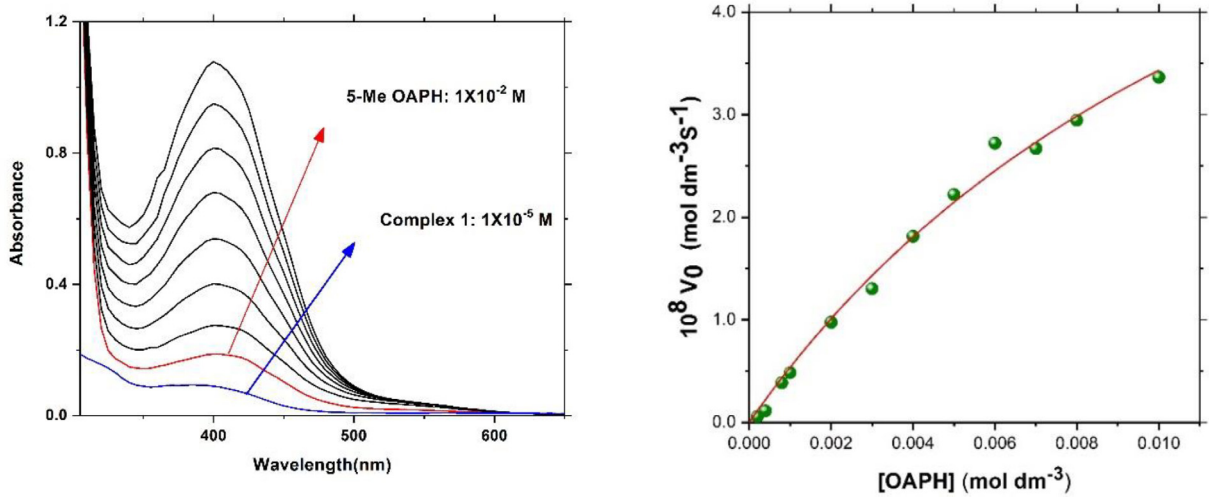

Fig. 5. UV–Vis spectral profile (left) and non-linear plot (right) of catalytic oxidation of 2-amino-5-methylphenol in dioxygen-saturated methanol at 25 °C catalysed by complex **1**.

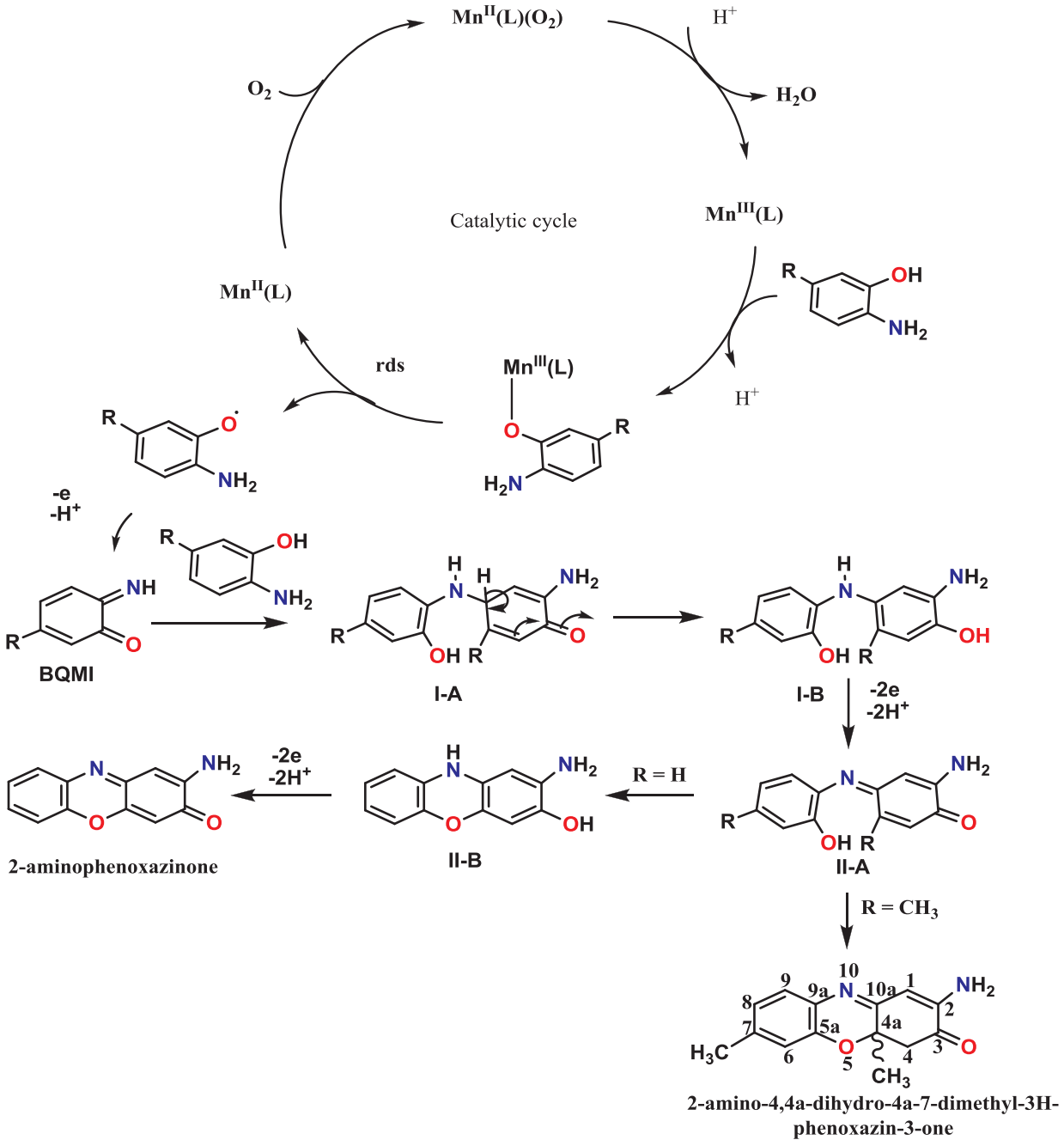

Scheme 2. Probable mechanistic pathway.

presented in supplementary section (Fig. S17(a)–S17(n)).

3.8.3. Probable mechanism and catalytic efficiency

Both rate saturation kinetics and the mass spectrometry studies suggest that the catalytic reactivity proceeds through the formation of a stable complex-substrate aggregate. As the present manganese complex is only four coordinated and thus substrate binding is quite probable. It is well known that the oxidation reactions catalysed by the manganese complexes proceed through the redox shuttling between the different oxidation states of manganese especially in between Mn(III) and Mn(II) [29h,57]. It is also obvious that the interactions of both the substrate and molecular dioxygen with the metal centre are important steps in the catalytic cycle exhibiting oxidase activity. From the mass spectrometry study, it is clear that both the dioxygen and substrate individually form stable adducts with the mental centres. However, the mass spectrometry study does not support the formation of any adduct in which both the substrate and dioxygen simultaneously bonded to the mental centre, therefore indicating that such an intermediate may not be a probable one in the present system, although it has been observed in many reported model complexes with different transition metals [29h,58]. Now we are at the right position to propose the most possible mechanism through which the present complex showing phenoxazinone synthase activity. At the first step of which the metal centre activates the dioxygen which thereafter oxidises Mn(II) to Mn(III) and itself reduces to H_2O. At the next step OAPH forms a complex-substrate aggregate which thereafter through redox transformation generates *o*-amninophenolate monoradical with regeneration of Mn(II)L. This OAP radical might be converted into *o*-benzoquinone monoamine (BQMI) in several ways including self-disproportionation reaction. Finally, 2-aminophenoxazin-3-one is produced through several oxidative

dehydrogenation processes involving OAPH, O_2, and BQMI as shown in Scheme 2.

Remarkably, intermediate II-B, shown in Scheme 2, was eventually detected in the mass spectrum of the complex in presence of excess substrate, thereby validating the said scheme. Two steps in the catalytic cycles i.e., dioxygen activation and the redox transformation of the complex-substrate aggregate leading to the generation of the OAP radicals are deserved to be special mention as either of them could be the rate limiting step of the catalytic cycle. The rate saturation kinetics with the varying substrate concentrations clearly justifies the involvement of the substrate in the rate determining step i.e., the later one. We should keep in mind that the different aggregates identified in the ESI-MS spectra may not necessarily mirror the real intermediate in the catalytic cycle because such aggregates may be formed *in situ* because of the relative stability when compared to the other cationic species in the time scale of ESI-MS spectrum. Therefore, although we have not observed any peak related to both substrate and dioxygen bound metal complex in the ESI-MS spectrum, the existence of such intermediate cannot be ruled out in the solution phase. In such a situation both substrate and dioxygen bound metal complex could be involved in the rate determining step. In order to get better insight into the mechanistic pathway we have measured the reaction kinetics in an identical condition but in different dioxygen concentrations. Remarkably, the initial rate of the reactions of all the cases found comparable, which clearly indicates that dioxygen does not involved in the rate determining step. Now it become clear that dioxygen rapidly oxidizes Mn(II) to Mn(III) in the catalytic cycle and itself reduces to water, and this process is so fast that the formation of both the substrate and dioxygen bound metal complex become least possible. A brief literature survey has been made and presented in Table S4. Table S4 exemplifies the k_{cat} values for the oxidation of OAPH by earlier reported catalyst transition metal complexes [29,59]. It clearly suggests that complex **1** exhibits moderate catalytic activity towards OAPH oxidation, but the reactivity of the present complex is somewhat lower than the recently published similar Mn(III)-salen type complex [29h]. The lower redox flexibility of the present complex as suggested by the cyclic voltammetric study, associated with the requirement of high reorganization energy for the structural change of the complex, is responsible for slightly lower activity. Like *o*-aminophenol, the catalytic oxidation of 2-amino-5-methylphenol proceeds through the identical pathway in which methyl substitution does not inhibit the formation of a stable complex-substrate aggregate as supported by the mass spectrometry and rate saturation kinetics. Interestingly, the presence of methyl substation in the benzene ring favours the substrate oxidation as indicated by the turn over numbers and these results also support the intramolecular electron transfer between the substrate and metal centre in the rate determining step. Moreover, the methyl substitution does not inhibit the coupling of two aminophenols, but the final dehydrogenation step was blocked by the methyl substitution, leading to the formation of dihydro-phenoxazinone chromophore as a final product (see Scheme 2).

4. Conclusion

A novel flattened tetrahedral Mn(II) complex has been synthesized using a very well-known Schiff-base ligand, H_2L. Probably this is the first example of flattened tetrahedral Mn(II) salen type of Schiff base complex. The propylenic linker in the ligand provides adequate flexibility so that such an uncommon binding mode of the salen type Schiff base ligand become possible. This complex is found as an efficient functional model for phenoxazinone synthase. Although the metal center interacts individually with dioxygen and substrate, the simultaneous coordination of both of them can be ruled out as suggested by both mass spectral study and kinetic studies with different dioxygen concentrations. Furthermore, the methyl substitution does not inhibit the coordination of the substrate to the metal centre and the coupling of the methyl-substituted *o*-aminophenol, but the final dehydrogenation step was blocked by the methyl substitution.

Declaration of Competing Interest

The authors declare that they have no known competing financial interests or personal relationships that could have appeared to influence the work reported in this paper

Acknowledgments

A. S. gratefully acknowledges the financial support of this work by the DST, India (Sanction No. SB/FT/CS-102/2014, dated- 18.07.2015. A. P. also gratefully acknowledges the financial support of this work by the University Grant Commission, India (Sanction no. F.PSW-229/15-16(ERO)).

Appendix A. Supplementary data

CCDC 1403382 contains the supplementary crystallographic data for complex **1**. This data can be obtained free of charge via http://www.ccdc.cam.ac.uk/conts/retrieving.html, or from the Cambridge Crystallographic Data Centre, 12 Union Road, Cambridge CB2 1EZ, UK; fax: (+44) 1223-336-033; or email: deposit@ccdc.cam.ac.uk. Supplementary data to this article can be found online at https://doi.org/10.1016/j.ica.2019.119176.

References

[1] A. Willing, H. Follman, G. Auling, Eur. J. Biochem. 170 (1988) 603–611.
[2] M.U. Triller, W.-Y. Hsieh, V.L. Pecoraro, A. Rompel, B. Krebs, Inorg. Chem. 41 (2002) 5544–5554.
[3] G. Gasser, I. Ott, N. Metzler-Nolte, J. Med. Chem. 54 (2011) 3–25.
[4] N. Mitic, C.J. Noble, L.R. Gahan, G.R. Hanson, G. Schenk, J. Am. Chem. Soc. 131 (2009) 8173–8179.
[5] V.V. Barynin, M.M. Whittaker, S.V. Antonyuk, V.S. Lamzin, P.M. Harrison, P.J. Artymiuk, J.W. Whittaker, Structure 9 (2001) 725–738.
[6] S.V. Antonyuk, W.R. Melik-Adamiyan, V.R. Popov, V.S. Lamzin, P.D. Hempstead, P.M. Harrison, P.J. Artymiuk, V.V. Barynin, Crystallogr. Rep. 45 (2000) 105–116.
[7] V.V. Barynin, P.D. Hempstead, A.A. Vagin, S.V. Antonyuk, W.R. Melik-Adamiyan, V.S. Lamzin, P.M. Harrison, P.J. Artymiuk, J. Inorg. Biochem. 67 (1997) 196.
[8] V.K. Yachandra, V.J. DeRose, M.J. Latimer, I. Mukerji, K. Sauer, M.P. Klein, Science 260 (1993) 675–679.
[9] M. Sundaramoorthy, K. Kishi, M.H. Gold, T.L. Poulos, J. Biol. Chem. 269 (1994) 32759–32767.
[10] S.V. Ley (Ed.), Comprehensive Organic Synthesis: Selectivity, Strategy and Efficiency in Modern Organic Chemistry, vol. 7, Elsevier, 1992.
[11] R.A. Sheldon, J.K. Kochi, Metal-Catalyzed Oxidations of Organic Compounds, Academic Press, New York, 1981.
[12] B. Cornils, Green Chemistry and Catalysis by Roger A. Sheldon, Isabel Arends and Ulf Hanefeld, Wiley-VCH, Weinheim, 2007.
[13] K.M. Gligorich, M.S. Sigman, Chem. Commun. (2009) 3854–3867.
[14] J. Piera, J.E. Backvall, Angew. Chem. Int. Ed. 47 (2008) 3506–3523.
[15] S.S. Stahl, Science 309 (2005) 1824–1826.
[16] T. Punniyamurthy, S. Velusamy, J. Iqbal, Chem. Rev. 105 (2005) 2329–2363.
[17] S.S. Stahl, Angew. Chem. Int. Ed. 43 (2004) 3400–3420.
[18] T. Funabiki (Ed.), Dioxygenases in Catalysis by Metal Complexes, Oxygenases and Model Systems, Kluwer Academic, Dordrecht, 1997, p. 19.
[19] J.P. Klinman, J. Biol. Inorg. Chem. 16 (2001) 1–13.
[20] I. Bertini, H.B. Gray, S.J. Lippard, J.S. Valentine (Eds.), Dioxygen Reactions in Bioinorganic Chemistry, University Science Books, Sausalito, 1994, p. 253.
[21] The chemistry and activation of dioxygen species (O2, O2– and H2O2) in biology, in: A.E. Martell, D.T. Sawyer, (Eds.), Oxygen Complexes and Oxygen Activation by Transition Metals, Plenum, New York, 1988, p. 131.
[22] E. Katz, H. Weissbach, J. Biol. Chem. 237 (1962) 882–886.
[23] (a) C.E. Barry III, P.G. Nayar, T.P. Begley, Biochemistry 28 (1989) 6323–6333; (b) C.E. Barry III, P.G. Nayar, T.P. Begley, J. Am. Chem. Soc. 110 (1988) 3333–3334.
[24] A.W. Smith, A. Camara-Artigas, M. Wang, J.P. Allen, W.A. Francisco, Biochemistry 45 (2006) 4378–4387.
[25] S.K. Dey, A. Mukherjee, Coord. Chem. Rev. 310 (2016) 80–115.
[26] V. Alexander, Chem. Rev. 95 (1995) 273–342.
[27] (a) D.E. Fenton, H. Okawa, Chem. Berl. 130 (1997) 433–435; (b) S.R. Collinson, D.E. Fenton, Coord. Chem. Rev. 148 (1996) 19–40; (c) D.E. Fenton, Pure Appl. Chem. 58 (1986) 1437–1444.
[28] S. Banerjee, A. Bauza, A. Frontera, A. Saha, RSC Adv. 6 (2016) 39376–39386.
[29] (a) P. Chakraborty, S. Majumder, A. Jana, S. Mohanta, Inorg. Chim. Acta 410 (2014) 65–75;

(b) S. Majumder, S. Hazra, S. Dutta, P. Biswas, S. Mohanta, Polyhedron 28 (2009) 2473–2479;
(c) P. Kar, P.M. Guha, M.G.B. Drew, T. Ishida, A. Ghosh, Eur. J. Inorg. Chem. (2011) 2075–2085;
(d) P. Kar, R. Biswas, M.G.B. Drew, A. Frontera, A. Ghosh, Inorg. Chem. 51 (2012) 1837–1851;
(e) S. Naiya, S. Biswas, M.G.B. Drew, C.J. Gomez-García, A. Ghosh, Inorg. Chem. 51 (2012) 5332–5341;
(f) P. Seth, S. Giri, A. Ghosh, Dalton Trans. 44 (2015) 12863–12870;
(g) P. Seth, M.G.B. Drew, A. Ghosh, J. Mol. Catal. A: Chem. 365 (2012) 154–161;
(h) S. Banerjee, P. Brandão, A. Bauzá, A. Frontera, M. Barceló-Oliver, A. Panja, A. Saha, New J. Chem. 41 (2017) 11607–11618.
[30] M.R. Chapman, S.E. Henkelis, N. Kapur, B.N. Nguyen, C.E. Willans, ChemistryOpen 5 (2016) 351–356.
[31] (a) J. Delaunay, R.P. Hugel, Inorg. Chem. 25 (1986) 3957–3961;
(b) C. Bucher, E. Duval, J.-M. Barbe, J.-N. Verpeaux, C. Amatore, R. Guilard, L.L. Pape, J. Latour, S. Dahaoui, C. Lecomte, Inorg. Chem. 40 (2001) 5722–5726;
(c) G. Berggren, P. Huang, L. Eriksson, M.F. Anderlund, Appl. Magn. Reson. 36 (2009) 9–24;
(d) C.C. Xue, H.Y. Zhang, D.P. Zhang, Russ. J. Coord. Chem. 43 (2017) 260–266;
(e) S. Xu, D. Wei, Asian J. Chem. 27 (2015) 3404–3406.
[32] G.M. Sheldrick, SAINT, Version 6.02, SADABS, Version 2.03, Bruker AXS Inc., Madison, Wisconsin, 2002.
[33] G.M. Sheldrick, SADABS: Software for Empirical Absorption Correction, University of Gottingen, Institute fur Anorganische Chemieder Universitat, Gottingen, Germany, (1999–2003).
[34] (a) G.M. Sheldrick, SHELXL-2017/1, Program for the Solution of Crystal Structures, University of Göttingen, Germany, 2017;
(b) G.M. Sheldrick, Acta Crystallogr. C 71 (2015) 3–8.
[35] M.G.B. Drew, R.N. Prasad, R.P. Sharma, Acta Crystallogr. C 41 (1985) 1755.
[36] M.J. Frisch, G.W. Trucks, H.B. Schlegel, G.E. Scuseria, M.A. Robb, J.R. Cheeseman, G. Scalmani, V. Barone, B. Mennucci, G.A. Petersson, H. Nakatsuji, M. Caricato, X. Li, H.P. Hratchian, A.F. Izmaylov, J. Bloino, G. Zheng, J.L. Sonnenberg, M. Hada, M. Ehara, K. Toyota, R. Fukuda, J. Hasegawa, M. Ishida, T. Nakajima, Y. Honda, O. Kitao, H. Nakai, T. Vreven, J.A. Montgomery Jr., J.E. Peralta, F. Ogliaro, M. Bearpark, J.J. Heyd, E. Brothers, K.N. Kudin, V.N. Staroverov, R. Kobayashi, J. Normand, K. Raghavachari, A. Rendell, J.C. Burant, S.S. Iyengar, J. Tomasi, M. Cossi, N. Rega, J.M. Millam, M. Klene, J.E. Knox, J.B. Cross, V. Bakken, C. Adamo, J. Jaramillo, R. Gomperts, R.E. Stratmann, O. Yazyev, A.J. Austin, R. Cammi, C. Pomelli, J.W. Ochterski, R.L. Martin, K. Morokuma, V.G. Zakrzewski, G.A. Voth, P. Salvador, J.J. Dannenberg, S. Dapprich, A.D. Daniels, Ö. Farkas, J.B. Foresman, J.V. Ortiz, J. Cioslowski, D.J. Fox, GAUSSIAN09, Revision D.01, Gaussian Inc., Wallingford, CT, 2009.
[37] A.D. Becke, J. Chem. Phys. 98 (1993) 5648–5652.
[38] C. Lee, W. Yang, R.G. Parr, Phys. Rev. B 37 (1988) 785–789.
[39] P.J. Hay, W.R. Wadt, J. Chem. Phys. 82 (1985) 270–283.
[40] W.R. Wadt, P.J. Hay, J. Chem. Phys. 82 (1985) 284–298.
[41] P.J. Hay, W.R. Wadt, J. Chem. Phys. 82 (1985) 299–310.
[42] G.A. Petersson, A. Bennett, T.G. Tensfeldt, M.A. Al-Laham, W.A. Shirley, J. Mantzaris, J. Chem. Phys. 89 (1988) 2193–2218.
[43] G.A. Petersson, M.A. Al-Laham, J. Chem. Phys. 94 (1991) 6081–6090.
[44] R. Bauernschmitt, R. Ahlrichs, Chem. Phys. Lett. 256 (1996) 454–464.
[45] R.E. Stratmann, G.E. Scuseria, M.J. Frisch, J. Chem. Phys. 109 (1998) 8218–8224.
[46] M.E. Casida, C. Jamorski, K.C. Casida, D.R. Salahub, J. Chem. Phys. 108 (1998) 4439–4449.
[47] V. Barone, M. Cossi, J. Phys. Chem. A 102 (1998) 1995–2001.
[48] M. Cossi, V. Barone, J. Chem. Phys. 115 (2001) 4708–4717.
[49] M. Cossi, N. Rega, G. Scalmani, V. Barone, J. Comput. Chem. 24 (2003) 669–681.
[50] N.M. O'Boyle, A.L. Tenderholt, K.M. Langner, J. Comput. Chem. 29 (2008) 839–845.
[51] S.K. Wolff, D.J. Grimwood, J.J. McKinnon, D. Jayatilaka, M.A. Spackman, Crystal Explorer 3.1, University of Western Australia, Perth, Australia, 2007.
[52] J.J. McKinnon, D. Jayatilaka, M.A. Spackman, Chem. Commun. (2007) 3814–3816.
[53] A.C. Sousa, M.C. Oliveira, L.O. Martins, M.P. Robalo, Green Chem. 16 (2014) 4127–4136.
[54] (a) T. Mathur, U.S. Ray, J.-C. Liou, J.S. Wu, T.-H. Lu, C. Sinha, Polyhedron 24 (2005) 739–746;
(b) H. Özay, M. Yıldız, H. Ünver, N.O. İskeleli, Synth. React. Inorg. Metal-org. Nano-metal Chem. 42 (2012) 872–877.
[55] (a) S. Sen, S. Mitra, D. Luneau, M. Salah El Fallah, J. Ribas, Polyhedron 25 (2006) 2737–2744;
(b) M. Maiti, D. Sadhukhan, S. Thakurta, E. Zangrando, G. Pilet, A. Bauzá, A. Frontera, B. Dede, S. Mitra, Polyhedron 75 (2014) 40–49.
[56] (a) S.K. Verma, V.K. Singh, Polyhedron 76 (2014) 1–9;
(b) S.A.A. Nami, K.S. Siddiqi, J. Chem. Res. (2006) 563–565.
[57] (a) A. Panja, RSC Adv. 4 (2014) 37085–37094;
(b) P. Seth, M.G.B. Drew, A. Ghosh, J. Mol. Catal. A: Chem. 365 (2012) 154–161;
(c) K.S. Banu, T. Chattopadhyay, A. Banerjee, M. Mukherjee, S. Bhattacharya, G.K. Patra, E. Zangrando, D. Das, Dalton Trans. (2009) 8755–8764.
[58] (a) J. Adhikary, A. Chakraborty, S. Dasgupta, S.K. Chattopadhyay, R. Kruszynski, A. Trzesowska-Kruszynska, S. Stepanović, M. Gruden-Pavlović, M. Swart, D. Das, Dalton Trans. 45 (2016) 12409–12422;
(b) A. Panja, N.Ch. Jana, Paula Brandaõ, New J. Chem. 41 (2017) 9784–9795;
(c) A. Panja, M. Shyamal, A. Saha, T.K. Mandal, Dalton Trans. 43 (2014) 5443–5452.
[59] (a) A. Panja, P. Guionneau, Dalton Trans. 42 (2013) 5068–5075;
(b) A. Panja, Polyhedron 80 (2014) 81–89;
(c) J. Kaizer, G. Baráth, R. Csonka, G. Speier, L. Korecz, A. Rockenbauer, L. Párkányi, J. Inorg. Biochem. 102 (2008) 773–780;
(d) A. Panja, RSC Adv. 3 (2013) 4954–4963;
(e) M. Szávuly, R.R. Csonka, G. Speier, R. Barabás, M. Giorgi, J. Kaizer, J. Mol. Catal. A: Chem. 392 (2014) 120–126;
(f) A. Panja, Polyhedron 79 (2014) 258–268;
(g) R. Bakshi, R. Kumar, P. Mathur, Catal. Commun. 17 (2012) 140–145;
(h) M.R. Maurya, S. Sikarwar, T. Joseph, S.B. Halligudi, J. Mol. Catal. A: Chem. 236 (2005) 132–138.